Journal of Power Sources 196 (2011) 3523–3529

Contents lists available at ScienceDirect

Journal of Power Sources

journal homepage: www.elsevier.com/locate/jpowsour

Carbon-supported Pd–Pt cathode electrocatalysts for proton exchange membrane fuel cells

Yongfu Tang[a,b], Huamin Zhang[a,*], Hexiang Zhong[a], Ting Xu[a,b], Hong Jin[a,b]

[a] Lab of PEMFC Key Materials and Technologies, Dalian Institute of Chemical Physical, Chinese Academy of Sciences, Dalian 116023, China
[b] Graduate School of Chinese Academy of Sciences, Beijing 100039, China

ARTICLE INFO

Article history:
Received 25 November 2010
Accepted 9 December 2010
Available online 21 December 2010

Keywords:
Proton exchange membrane fuel cells
Oxygen reduction reaction
Carbon-supported Pd–Pt alloy
Low-platinum electrocatalyst

ABSTRACT

A series of carbon-supported Pd–Pt alloy (Pd–Pt/C) catalysts for oxygen reduction reaction (ORR) with low-platinum content are synthesized via a modified sodium borohydride reduction method. The structure of as-prepared catalysts is characterized by powder X-ray diffraction (XRD) and transmission electron microscope (TEM) measurements. The prepared Pd–Pt/C catalysts with alloy form show face-centered-cubic (FCC) structure. The metal particles of Pd–Pt/C catalysts with mean size of around 4–5 nm are uniformly dispersed on the carbon support. The electrocatalytic activities for ORR of these catalysts are investigated by rotating disk electrode (RDE), cyclic voltammetry (CV), single cell measurements and electrochemical impedance spectra (EIS) measurements. The results suggest that the electrocatalytic activities of Pd–Pt/C catalysts with low platinum are comparable to that of the commercial Pt/C with the same metal loading. The maximum power density of MEA with a Pd–Pt/C catalyst, the Pd/Pt mass ratio of which is 7:3, is about 1040 mW cm^{-2}.

1. Introduction

Due to the high power density, high efficiency and low emissions, proton exchange membrane fuel cells (PEMFCs) are considered as a promising technique for portable power sources and electrical vehicles [1]. One of the major obstacles for the commercial application of PEMFCs is the extremely high cost of the platinum based catalysts [2]. Several strategies have been explored to reduce the Pt loading and enhance the utilization of Pt, one of which is alloying Pt with a second metal. Many researchers have demonstrated that Pt-based alloys with transitional metal exhibited much higher ORR activity than pure Pt [3–7]. However, the loss of transitional metal in acid condition, which greatly reduces the durability of catalysts, hinders the practical application of Pt–M (M = Fe, Co, Ni, Cr, etc.) catalysts [3,8–11]. Furthermore, the leaching out of metal ions would contaminate the proton exchange membrane and invalidate the fuel cell. Therefore, the development of low Pt catalyst with high activity and high durability in acidic condition becomes one of most important topic in PEMFC.

Palladium possesses a similar valence electronic configuration and lattice constant to platinum [12]. The stability of palladium in acidic condition is comparable to platinum [13,14]. Recent reports have shown that Pt-rich carbon-supported Pt–Pd alloys showed high activity and durability for ORR. Li et al. [15] reported that a carbon-supported Pt_3Pd catalyst prepared by the polyol process showed a slightly higher ORR activity compared with carbon-supported Pt. He et al. [16] synthesized carbon supported Pt–Pd alloys with different atomic ratios, among which the Pt_2Pd/C catalysts showed a comparative activity to Pt/C. However, the particle size of carbon-supported Pd–Pt alloys increases remarkably with the increasing of Pd content [13,15,17,18]. Furthermore, the activities of these carbon-supported Pd–Pt alloys with high Pd content (atom ratio Pd/Pt > 1) are much lower than that of Pt/C [15,16,18].

To further decrease the cost of PEMFC catalyst, a series of carbon-supported Pd–Pt alloys catalysts with high Pd content were synthesized by modified sodium borohydride reduction method in this paper. Similar with our previous work, this method used ammonia as ligand of the precursor and sodium borohydride as reduction reagent [19]. The obtained particles of Pd–Pt catalysts are uniformly dispersed on the carbon support, and the mean particle size of them is in the range of 4–5 nm which is the optimized particle size range for the ORR [20]. The particle size of Pd–Pt alloys keeps constant with the increasing of Pd content due to the instantaneous reduction of the precursor and the protection of ammonia. To investigate the effect of Pd/Pt ratio on the catalysts structure and the catalytic activity for ORR, Pd–Pt/C catalysts with different Pd/Pt mass ratios were prepared and investigated in detail.

* Corresponding author. Tel.: +86 411 84379072; fax: +86 411 84665057.
E-mail address: zhanghm@dicp.ac.cn (H. Zhang).

0378-7753/$ – see front matter © 2010 Elsevier B.V. All rights reserved.
doi:10.1016/j.jpowsour.2010.12.048

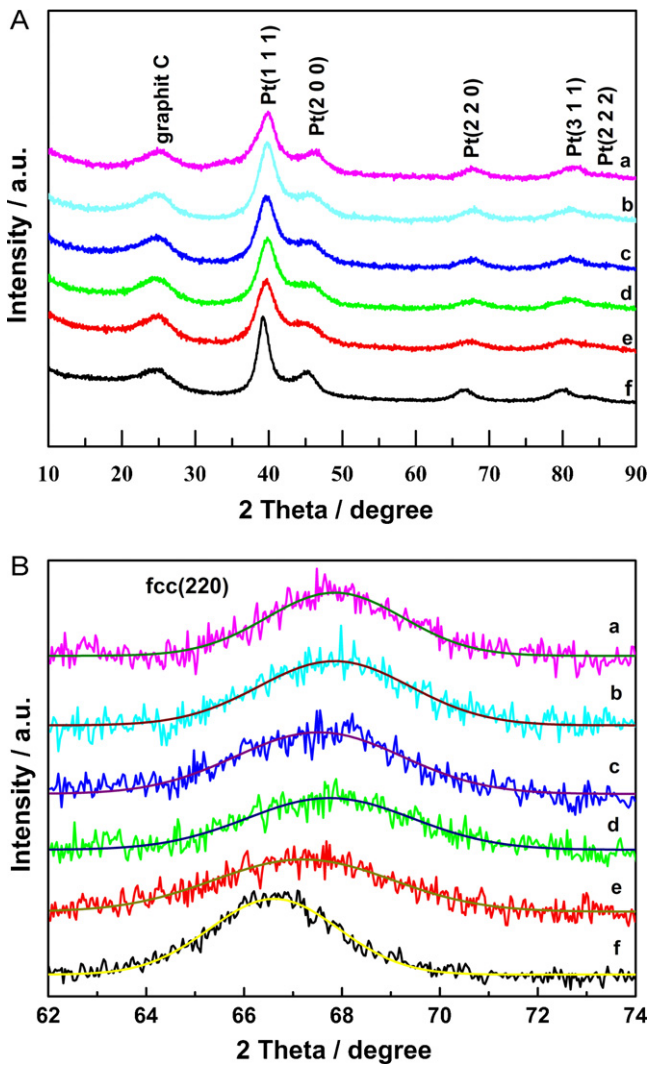

Fig. 1. (A) Powder XRD patterns of the (a) JM Pt/C, (b) $Pd_{12}Pt_8$/C, (c) $Pd_{14}Pt_6$/C, (d) $Pd_{16}Pt_4$/C, (e) $Pd_{18}Pt_2$/C, and (f) Pd/C catalysts. (B) Detailed lines and Gaussian fitted lines of fcc (2 2 0) peaks powder XRD patterns of the (a) JM Pt/C, (b) $Pd_{12}Pt_8$/C, (c) $Pd_{14}Pt_6$/C, (d) $Pd_{16}Pt_4$/C, (e) $Pd_{18}Pt_2$/C, and (f) Pd/C catalysts.

2. Experimental

2.1. Catalysts preparation

Carbon-supported Pd–Pt alloys (Pd–Pt/C) with different Pd/Pt mass ratios were synthesized by the modified sodium borohydride reduction method reported in our previous work [19]. The preparation process is described in detail as follows: Vulcan XC-72 carbon black was used as the support. $PdCl_2$ dissolved in hydrochloric acid and H_2PtCl_6 dissolved in deionized water were used as the precursors of Pd and Pt, respectively. The Pd/Pt mass ratios were ranged from 9:1 to 6:4 and the total metal loading was kept as 20 wt.%. The designed amount of $PdCl_2$ in hydrochloric acid was mixed with the mixture of deionized water and ethylene glycol. Then 1 mL ammonia (25 wt.%) was added to the mixed solution under continuously stirring. When the color of the solution changed from yellow to colorless, the designed amount of H_2PtCl_6 was introduced into the solution. Afterward, excessive $NaBH_4$ solution was added dropwisely to reduce these precursors. The catalysts were obtained after centrifuging, washing and drying the mixture. The Pd–Pt/C catalysts with different Pd/Pt mass ratios ranged from 9:1 to 6:4 were denoted as $Pd_{18}Pt_2$/C, $Pd_{16}Pt_4$/C, $Pd_{14}Pt_6$/C and $Pd_{12}Pt_8$/C, respectively. The Pd/C catalyst reported in our previous paper [19] was used to compare with these Pd–Pt/C catalysts.

2.2. Physicochemical characterizations

Powder X-ray diffraction (XRD) analysis was conducted to confirm the crystalline structures of the Pd–Pt/C catalysts and commercial Pt/C with PANalytical X'Pert-Pro powder X-ray diffractometer using Ni-filtered Cu Kα radiation (λ = 1.54056 Å). The XRD patterns were recorded over a 2θ range of 10–90° at the step size of 0.033°. The (2 2 0) peak of the face-centered cubic (fcc) reflection patterns was fitted to Gaussian line shapes on a linear background. The average crystallite size and the lattice parameters were evaluated by Scherrer formula and Bragg's equation [21,22], respectively.

Transmission electron microscope (TEM) tests were recorded on a JEOL JEM-2000EX microscope operating at 120 kV. The Pd–Pt/C catalyst was placed in a vial containing ethanol, and then ultrasonically agitated to form homogeneous slurry. A drop of the slurry was dispersed on a holey amorphous carbon film on a Cu grid for analyses. Particle size distribution for the nanocomposite materials was obtained by randomly measuring 200 particles from bright-field micrographs. The mean particle size d_m was calculated with the following formula [23]

$$d_m = \frac{\sum_i n_i d_i}{\sum_i n_i} \quad (1)$$

where n_i is the number of particles and d_i is the diameter of the particle with the number of n_i.

2.3. Electrochemical characterizations

Electrochemical measurements were performed on CHI 600 electrochemical station (CH Corporation, USA) with an RDE system (EG&G model 636). A standard three-electrode electrochemical cell was used as the measurement system. A large-area Pt foil (3 cm^2) and a saturated calomel electrode (SCE) were served as the counter electrode and the reference electrode, respectively. All the electrode potentials in this paper were quoted to reversible hydrogen electrode (RHE). The working electrode was prepared as follows: 5 mg of catalyst was mixed with 1 mL isopropyl alcohol and 50 μL Nafion solution (5 wt.%, Du Pont Corp.). Then the mixture was homogenized in an ultrasonic bath for 30 min to obtain ink slurry. 10 μL of the slurry was dispersed on the surface of the glassy carbon electrode (area: 0.1256 cm^2) and dried in the air to obtain a thin film catalyst layer. Cyclic voltammetry (CV) measurements were conducted in the high purity N_2 saturated 0.5 M H_2SO_4 solution and carried out between −0.01 V and 1.14 V versus RHE at 50 mV s^{-1} scan rate. The polarization curves were obtained in the potential range of 0.24–1.09 V versus RHE with the applied scan rate of 5 mV s^{-1}. The disk electrode rotation speed is 1600 rpm. Prior to the RDE test, the H_2SO_4 solution was saturated with high pure O_2.

2.4. Fabrication of membrane electrode assembly (MEA) and single-cell test

The fabrication of electrodes and MEAs was referred to in our previous work [24]. The process in detail is described as follows: the designed amount of catalysts, 5 wt.% Nafion solution (Du Pont Corp.) and isopropyl alcohol were mixed together to form homogeneous slurry. The slurry was brushed on the surface of wet-proofed carbon gas diffusion layer (SGL, 6% PTFE). The total metal loading of Pd and Pt on the electrode was about 0.4 mg cm^{-2} and the dry Nafion loading was also about 0.4 mg cm^{-2}. The commercial Pt/C (20 wt.%, Johnson Matthey Corp.) cathode was

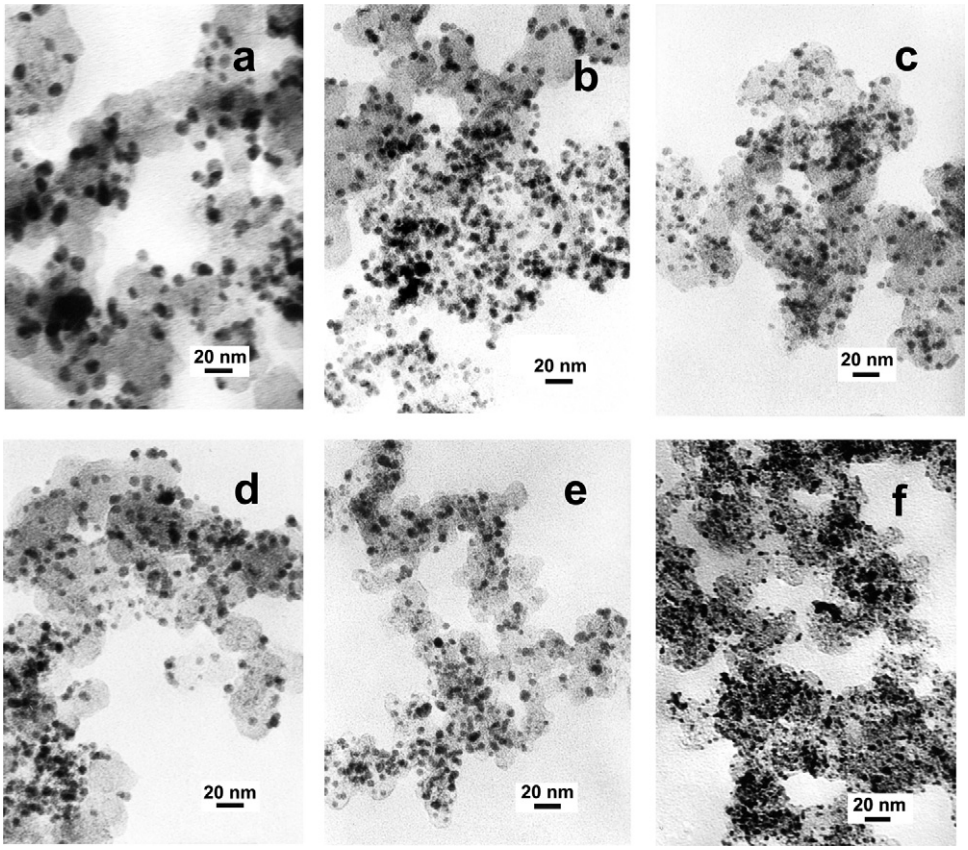

Fig. 2. TEM images of (a) Pd/C, (b) $Pd_{18}Pt_2$/C, (c) $Pd_{16}Pt_4$/C, (d) $Pd_{14}Pt_6$/C, (e) $Pd_{12}Pt_8$/C and (f) JM Pt/C catalysts.

prepared by the same process and same loading for comparing. The anode adopted the commercial 28.4% Pt/C catalyst (TKK Corp.) with Pt loading of 0.3 mg cm^{-2}. The dry Nafion loading in the anode was about 0.4 mg cm^{-2}. The MEAs were fabricated by hot-pressing the anode and the cathode to Nafion 212 membrane (50 μm, Du Pont Corp.) with a sandwich structure, the active area of which was about 5 cm^2. It was operated at 140 °C and 1 MPa for 1 min. The singe-cells were tested at 80 °C and 0.2 MPa with saturated humidification and fed with pure hydrogen and oxygen.

Electrochemical impedance spectra (EIS) of the cells were recorded using a KIKUSUI FC Impedance Meter KFM 2030 frequency-response analyzer. The anode of the single cell was used as the counter electrode and reference electrode, and the cathode was used as working electrode. The impedance spectra were measured at different current densities (100, 200 and 500 mA cm^{-2}) to investigate the electrochemical impedance of the single cell. The impedance spectra were measured by sweeping the frequency between the 10 kHz and 100 mHz range and recorded with logarithmic spacing.

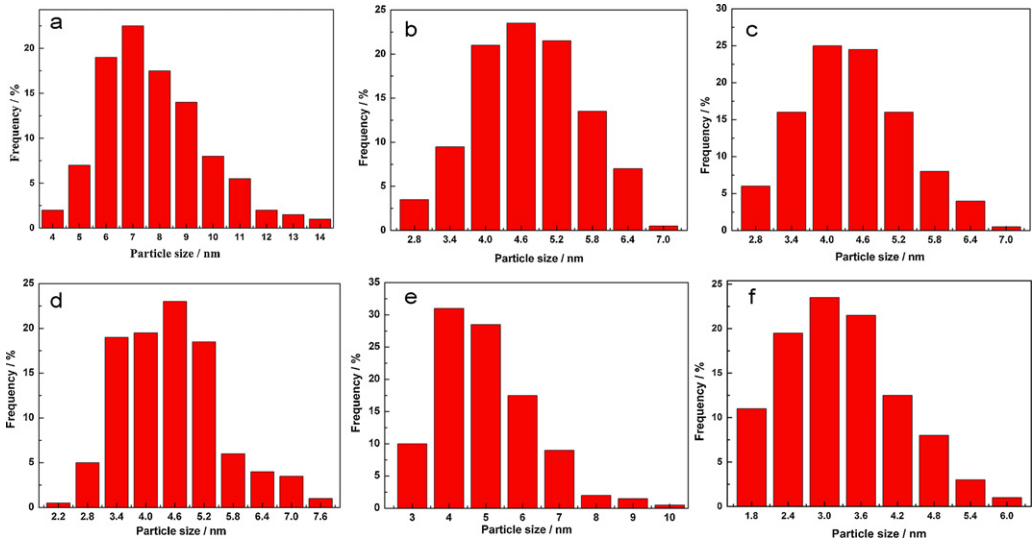

Fig. 3. Histograms of metal particle sizes of (a) Pd/C, (b) $Pd_{18}Pt_2$/C, (c) $Pd_{16}Pt_4$/C, (d) $Pd_{14}Pt_6$/C, (e) $Pt_{12}Pt_8$/C and (f) JM Pt/C catalysts.

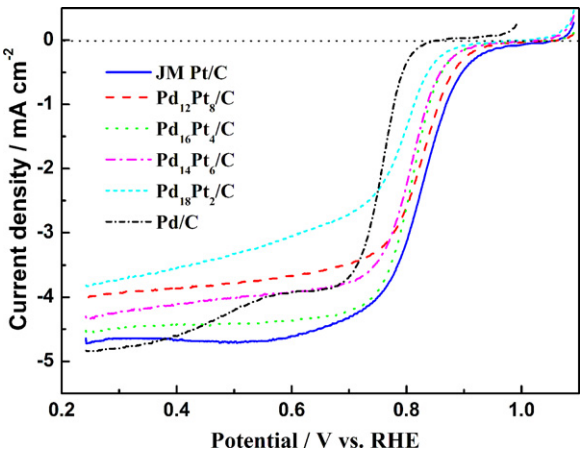

Fig. 4. Current-potential polarization curves for Pd–Pt/C catalysts, Pd/C and JM Pt/C in O_2-saturated 0.5 M H_2SO_4. Scan rate: 5 mV s^{-1}. Rotation speed: 1600 rpm.

3. Results and discussion

3.1. Physicochemical characterizations

Fig. 1A shows the XRD pattern of Pd–Pt/C catalysts. The commercial Pt/C catalyst (Johnson Matthey, 20 wt.% Pt/C) and the Pd/C catalyst reported in our previous work [19] are introduced for comparison. The diffraction peaks of Pd–Pt/C catalysts at about 40°, 46°, 68°, 81° and 86° are attributed to the (1 1 1), (2 0 0), (2 2 0), (3 1 1) and (2 2 2) planes of the face center cubic (FCC) structure of the Pd–Pt alloys. The mass ratio of Pd/Pt has a slight effect on the crystalline structure due to the similar crystalline structures of Pt and Pd. Diffraction peaks, which can be assigned to oxides or hydroxides of palladium and platinum, are not detected. This result suggests that palladium and platinum exist as metallic phases due to the strong reductive activity of sodium borohydride.

The mean metal crystalline size and lattice parameters of all the catalysts were calculated by Scherrer formula and Bragg's equation [21,22] with the (2 2 0) peaks. The detailed lines and Gaussian fitted lines of fcc (2 2 0) peaks of these catalysts are shown in Fig. 1B. The data of crystalline size and lattice parameters are listed in the Table 1. As seen in Table 1, the lattice parameters of all the carbon-supported Pd–Pt catalysts are in the range of JM Pt/C catalysts and Pd/C catalysts. This result indicates that Pd–Pt binary metal of the Pd–Pt/C catalysts exist as the alloy form. It may be attributed to the intense reductive activity of sodium borohydride which can mix the Pd and Pt at the level of atoms when they were reduced. The metal crystalline size of all the Pd–Pt/C catalysts is smaller than that of Pd/C and JM Pt/C catalysts. It is interesting that crystalline size of the metal nanoparticles is not increase with the increase of the Pd content, which is different from the report in the literatures [13,15,17,18]. The reason for the smaller crystalline size of the Pd–Pt/C catalysts with high Pd content may be attributed to the rapid reduction of Pd and Pt precursors and the protective effect of ammonia.

Fig. 2 shows the TEM images of the Pd–Pt/C, Pd/C and JM Pt/C catalysts. The corresponding particle size distribution histograms are shown in Fig. 3. The mean metal particle size of these catalysts calculated with Formula (1) is collected in Table 1. As seen in Fig. 2, the spherical metal particles of all the catalysts are uniformly dispersed on the carbon support. With the addition of low amount of platinum, the mean particle size of Pd–Pt/C catalysts decreases obviously. The mean particle sizes of $Pd_{18}Pt_2$/C, $Pd_{16}Pt_4$/C, $Pd_{14}Pt_6$/C, $Pd_{12}Pt_8$/C and JM Pt/C samples are 4.7 nm, 4.4 nm, 4.5 nm, 5.0 nm and 3.3 nm, respectively. The mean particle size of Pd/C sample is 7.8 nm which is nearly twice as large as that of Pd–Pt/C samples. Furthermore, the particle size distribution of Pd–Pt/C catalysts is narrower than that of Pd/C catalyst. For example, the particle sizes of $Pd_{18}Pt_2$/C and $Pd_{16}Pt_4$/C are narrowly distributed in the range between 2.5 nm and 7.3 nm, which is remarkably narrower than that of Pd/C catalyst, which is in the range of 3 nm and 15 nm. Interestingly, the mean particle size counted by TEM images of all the Pd–Pt/C catalysts is nearly twice as large as the crystalline size calculated by XRD patterns. This phe-

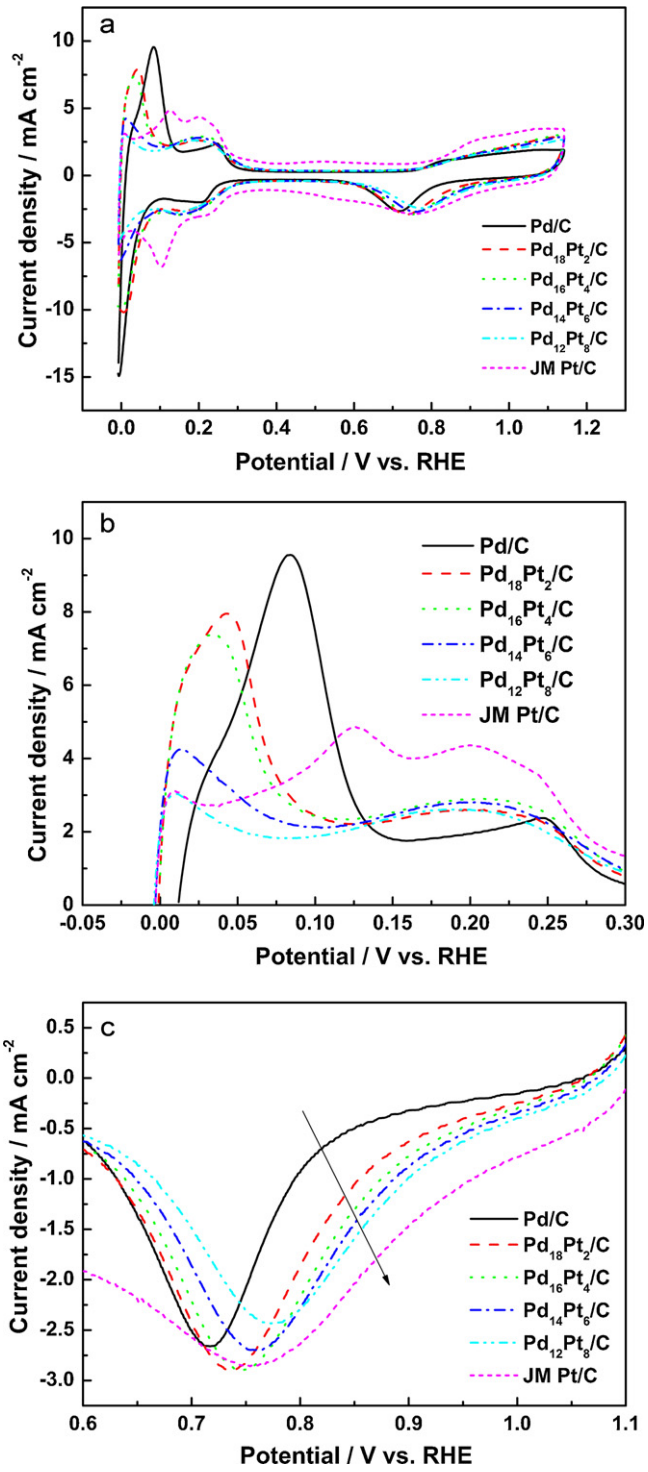

Fig. 5. Cyclic voltammograms (a) and the details of hydrogen region (b) and oxygen region (c) of Pd–Pt/C, Pd/C and JM Pt/C catalysts in N_2-saturated 0.5 M H_2SO_4 at room temperature, recorded at sweeping rate of 50 mV cm^{-2}.

Table 1
Date of lattice parameter, crystalline sizes and mean particle size of Pd–Pt/C, Pd/C and JM Pt/C catalysts.

Catalyst sample	Lattice parameter (nm)	Crystalline size (nm)	Mean particle size (nm)
Pd/C	0.3968	2.8	7.8
$Pd_{18}Pt_2$/C	0.3941	2.2	4.7
$Pd_{16}Pt_4$/C	0.3912	2.3	4.4
$Pd_{14}Pt_6$/C	0.3920	2.8	4.5
$Pd_{12}Pt_8$/C	0.3904	2.5	5.0
JM Pt/C	0.3902	2.9	3.3

Table 2
The electrochemical data of Pd–Pt/C, Pd/C and JM Pt/C catalysts.

	JM Pt/C	$Pd_{12}Pt_8$/C	$Pd_{14}Pt_6$/C	$Pd_{16}Pt_4$/C	$Pd_{18}Pt_2$/C	Pd/C
Onset potential (V)	1.06	1.06	1.06	1.03	1.01	0.86
i_k at 0.85 V (mA cm^{-2})	2.26	1.65	0.84	0.78	0.36	–
The half-wave potential $E^{1/2}$ (V)	0.825	0.822	0.807	0.802	0.777	0.749

nomenon mentioned is also observed and discussed in detail in our previous work [19].

3.2. Electrochemical characterizations

Fig. 4 displays the ORR polarization curves for Pd–Pt/C catalysts in O_2-saturated 0.5 M H_2SO_4 solution at room temperature. The polarization curves of Pd/C and commercial Pt/C catalysts are included for comparison. As seen in Fig. 4 and Table 2, the half-wave potentials of all the Pd–Pt/C catalysts are comparable to that of JM Pt/C catalyst but much higher than that of Pd/C catalyst. With the platinum content increasing, the ORR catalytical activities of Pd–Pt/C catalysts increase. When the amount of platinum is up to 4 wt.%, the catalytic activity for ORR is comparable to that of JM Pt/C. The high activity might be ascribed to the following two aspects: Firstly, the metal particles of Pd–Pt/C catalysts with small size are uniformly dispersed on the carbon support, which results in the high active surface area of the catalysts. Secondly, the synergic effect of Pd–Pt binary is beneficial for the dissociation of oxygen molecule [15,25–27], which can enhance the ORR.

Table 2 shows the electrochemical data of Pd–Pt/C, Pd/C and JM Pt/C catalysts. According to the thin-film rotating disk electrode theory [28], the apparent resistance ($1/i$) can be obtained from the kinetic resistance ($1/i_k$) and the limit diffusion resistance ($1/i_d$), with the following equation

$$\frac{1}{i} = \frac{1}{i_k} + \frac{1}{i_d} \quad (2)$$

where i, i_k and i_d are the apparent current density, the kinetic current density and diffusion limit current density, respectively. Eq. (2) could be converted to the following equation which is used to calculate the kinetic current density (i_k) [28].

$$i_k = \frac{i \cdot i_d}{i_d - i} \quad (3)$$

As seen in Table 2, the onset potential and i_k at 0.85 V of these Pd–Pt/C catalysts are comparable to those of JM Pt/C. The kinetic current density i_k at 0.85 V of $Pd_{12}Pt_8$/C and $Pd_{14}Pt_6$/C are 1.65 and 0.84 mA cm^{-2}, respectively, which are close to that of JM Pt/C (2.26 mA cm^{-2}). The results demonstrate that the intrinsic activities of Pd–Pt/C catalysts with low Pt content are comparable to that of JM Pt/C.

To investigate the possible electrochemical reaction of hydrogen and oxygen on the surface of catalysts, cyclic voltammograms measurements were carried out on Pd–Pt/C catalysts, JM Pt/C and Pd/C catalyst respectively in the potential range of −0.01 V and 1.14 V. Fig. 5a exhibits the CV curves of Pd–Pt/C catalysts, JM Pt/C and Pd/C catalyst. Fig. 5b and c shows the detailed information of hydrogen region (Fig. 5b) and oxygen region (Fig. 5c). As seen in hydrogen region, three peaks around 0 V, 0.13 V and 0.20 V of JM Pt/C can be attributed to hydrogen under-potential deposition (H_{upd}), hydrogen adsorption on Pt(1 1 0) plane and hydrogen adsorption on Pt(1 1 1) plane, respectively [29]. Two typical peaks attributed to the hydrogen under-potential deposition (H_{upd}) and hydrogen oxidation are observed round 0.08 V and 0.25 V [26]. The current density plateau of all these catalysts (between 0.3 V and 0.8 V) is attributed to the double layer current. The current densities in the double layer region of Pd–Pt/C catalysts are close to that of Pd/C catalyst and markedly lower than that of JM Pt/C. The positive and negative peaks in high potential region (above 0.7 V) are ascribed to the oxidation of metal and reduction of the corresponding metal oxide [30].

3.3. Performance of single cell and EIS spectra

The $Pd_{14}Pt_6$/C catalyst was selected to investigate its single cell performance due to its high ORR activity and low Pt loading. The performance of single cells at 80 °C with $Pd_{14}Pt_6$/C and JM Pt/C as cathode catalyst is shown in Fig. 6. The total metal loading of both cathodes is 0.4 mg cm^{-2}. The open circuit voltages of MEAs with $Pd_{14}Pt_6$/C and JM Pt/C as cathode catalyst are 0.93 V and 0.97 V, respectively. During the low current density region (below 500 mA cm^{-2}), the cell voltage of $Pd_{14}Pt_6$/C cathode MEA is only 10–20 mV lower than that of JM Pt/C catalyst MEA at the

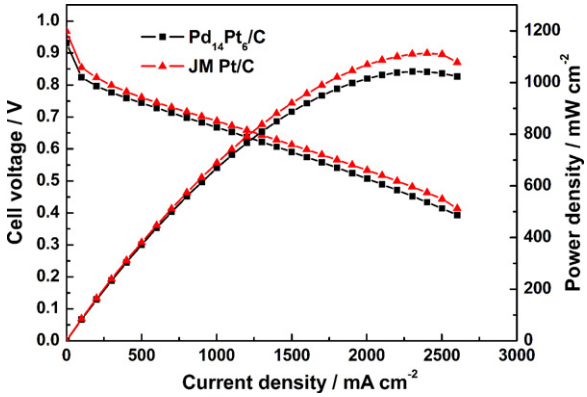

Fig. 6. Performances of single cells with the $Pd_{14}Pt_6$ and the JM Pt/C as the cathode catalysts at cell operating temperature of 80 °C. Anode: the commercial TKK 28.4 wt.% Pt/C with the Pt loading is 0.3 mg cm^{-2}. Total metal loading of cathode: 0.4 mg cm^{-2}. H_2/O_2 pressure: 0.2 MPa/0.2 MPa. Membrane: Nafion 212. Pure hydrogen and oxygen were put into the cell with saturated humidification.

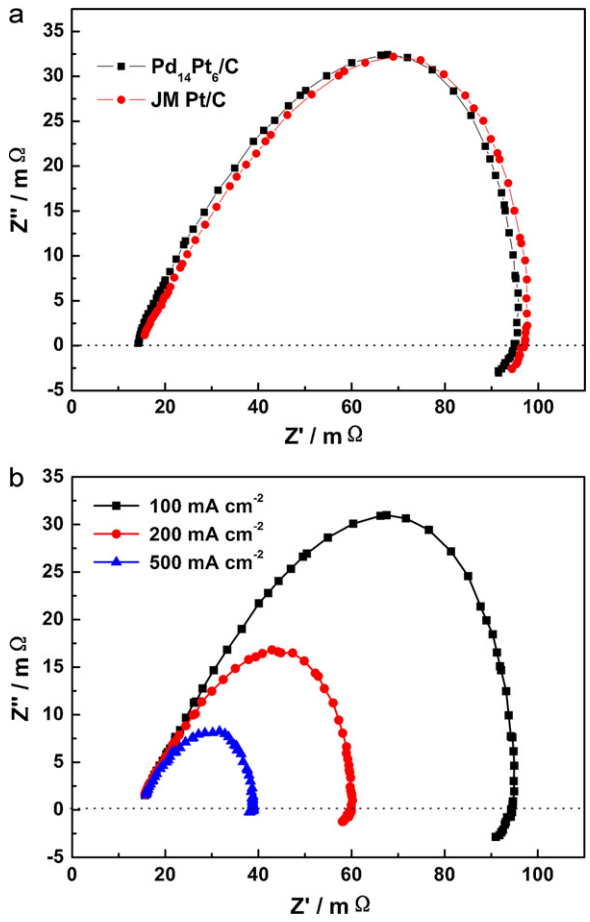

Fig. 7. (a) EIS of the PEM single cells with the $Pd_{14}Pt_6$/C and the JM Pt/C as the cathode catalysts and (b) EIS of the PEM single cells with the $Pd_{14}Pt_6$/C catalyst at different current density. The area of electrode was 5 cm^2.

same current density. The maximum power density of MEA with $Pd_{14}Pt_6$/C catalyst achieved 1040 mW cm^{-2} at the current density of 2300 mA cm^{-2}, which is only 70 mW cm^{-2} lower than the maximum power density of MEA with JM Pt/C catalyst. It is clear that the performance of MEA with $Pd_{14}Pt_6$/C as cathode catalyst, in which the Pt loading of MEAs is only 0.12 mg cm^{-2}, is comparable to that of the MEA with JM Pt/C catalyst. Thus $Pd_{14}Pt_6$/C is a really good candidate to substitute the currently used platinum, which can dramatically decrease the cost of PEMFC.

Fig. 7 exhibits the EIS spectra of the single cells with $Pd_{14}Pt_6$/C and JM Pt/C catalysts (Fig. 7a) at the current density of 100 mA cm^{-2} and the EIS spectra of $Pd_{14}Pt_6$/C at different current densities (Fig. 7b). As shown in Fig. 7, the intersection of the real axis and the impedance at high frequency is attributed to the total ohmic resistances of the single cell. The larger loop of EIS spectra is ascribed to the charge-transfer resistance of the cathode oxygen reduction [31]. As seen in Fig. 7a, the total ohmic resistance and the charge-transfer resistance of the cathode of MEA with $Pd_{14}Pt_6$/C catalyst are very close to that of MEA with JM Pt/C catalyst, which is well agreement with the result of the ORR measurement and the performance of MEAs. Fig. 7b shows the EIS spectra of MEA with $Pd_{14}Pt_6$/C catalyst at different current density. The total ohmic resistance does not change with the increase of current densities, while the charge-transfer resistance of the cathode decreases with the increase of current density. It can be attributed to that the increasing current density in low polarization region can enhance the electrochemical kinetics of ORR [32].

4. Conclusion

In this study, a series of Pd–Pt/C catalyst with low platinum content were synthesized via modified sodium borohydride reduction method. The results demonstrate that the Pd–Pt binary metal exists as alloy form. The metal crystalline size of all the Pd–Pt/C catalysts is smaller than that of Pd/C and JM Pt/C catalysts, which may result in the high active surface area of the catalysts. The obtained particles of Pd–Pt alloys are uniformly dispersed on the carbon, the mean size of which is around 4–5 nm. The particle sizes of Pd–Pt alloys do not increase with Pd content increasing due to the instantaneous reduction of the precursor and the protection of ammonia. The electrochemical measurements indicate that the ORR activities of $Pd_{14}Pt_6$/C and $Pd_{12}Pt_8$/C catalysts are comparable to that of JM Pt/C catalyst. The high activity of Pd–Pt/C catalysts might be ascribed to the high active surface area of the catalysts and the synergic effect of Pd–Pt binary. The maximum power density of MEA with $Pd_{14}Pt_6$/C catalyst achieved at the current density of 2300 mA cm^{-2} is 1040 mW cm^{-2}, which is only 70 mW cm^{-2} lower than the maximum power density of MEA with JM Pt/C catalyst.

In summary, the Pd–Pt/C catalyst is a really good candidate to substitute the currently used platinum, which can dramatically decrease the cost of PEMFC. The study of Pd–Pt/C catalysts is signification for the commercial application of PEMFCs. Further effort should focus on the optimization of preparation process to improve the catalytic activity of Pd–Pt/C catalysts.

Acknowledgement

This work is partly supported by the National High Technology Research and Development Program of China (863 Program), No. 2009AA05Z114, No. 2008AA05Z106 and No. 2009AA034400.

References

[1] R.F. Service, Science 324 (2009) 1257–1259.
[2] W. Vielstich, A. Lamm, H.A. Gasteiger, Handbook of Fuel Cells: Fundamentals, Technology, Applications, vol. 3, Wiley, New York, 2003.
[3] W. Li, W. Zhou, H. Li, Z. Zhou, B. Zhou, G. Sun, Q. Xin, Electrochim. Acta 49 (2004) 1045–1055.
[4] T. Toda, H. Igarashi, M. Watanabe, J. Electroanal. Chem. 460 (1999) 258–262.
[5] H. Yang, W. Vogel, C. Lamy, N. Alonso-Vante, J. Phys. Chem. B 108 (2004) 11024–11034.
[6] V.R. Stamenkovic, B. Fowler, B.S. Mun, G. Wang, P.N. Ross, C.A. Lucas, N.M. Markovic, Science 315 (2007) 493–497.
[7] S. Chen, P.J. Ferreira, W. Sheng, N. Yabuuchi, L.F. Allard, Y. Shao-Horn, J. Am. Chem. Soc. 130 (2008) 13818–13819.
[8] K.T. Kim, J.T. Hwang, Y.G. Kim, J.S. Chung, J. Electrochem. Soc. 140 (1993) 31–36.
[9] K.T. Kim, Y.G. Kim, J.S. Chung, J. Electrochem. Soc. 142 (1995) 1531–1538.
[10] M.T. Paffett, J.G. Beery, S. Gottesfeld, J. Electrochem. Soc. 135 (1988) 1431–1436.
[11] M. Watanabe, K. Tsurumi, T. Mizukami, T. Nakamura, P. Stonehart, J. Electrochem. Soc. 141 (1994) 2659–2668.
[12] C. Lamy, Electrochim. Acta 29 (1984) 1581–1588.
[13] J. Yang, J.Y. Lee, Q. Zhang, W. Zhou, Z. Liu, J. Electrochem. Soc. 155 (2008) B776–B781.
[14] Z.-M. Zhou, Z.-G. Shao, X.-P. Qin, X.-G. Chen, Z.-D. Wei, B.-L. Yi, Int. J. Hydrogen Energy 35 (2010) 1719–1726.
[15] H. Li, G. Sun, N. Li, S. Sun, D. Su, Q. Xin, J. Phys. Chem. C 111 (2007) 5605–5617.
[16] W. He, J. Liu, Y. Qiao, Z. Zou, X. Zhang, D.L. Akins, H. Yang, J. Power Sources 195 (2010) 1046–1050.
[17] A.C. Garcia, V.A. Paganin, E.A. Ticianelli, Electrochim. Acta 53 (2008) 4309–4315.
[18] W. Wang, Q. Huang, J. Liu, Z. Zou, Z. Li, H. Yang, Electrochem. Commun. 10 (2008) 1396–1399.
[19] Y. Tang, H. Zhang, H. Zhong, Y. Ma, Int. J. Hydrogen Energy (2010), doi:10.1016/j.ijhydene.2010.09.037.
[20] M.S. Wilson, F.H. Garzon, K.E. Sickafus, S. Gottesfeld, J. Electrochem. Soc. 140 (1993) 2872–2877.
[21] Z. Liu, L.M. Gan, L. Hong, W. Chen, J.Y. Lee, J. Power Sources 139 (2005) 73–78.
[22] V. Radmilovic, H.A. Gasteiger, P.N. Ross, J. Catal. 154 (1995) 98–106.
[23] I. Dobrosz, K. Jiratova, V. Pitchon, J.M. Rynkowski, J. Mol. Catal. A Chem. 234 (2005) 187–197.

[24] G. Liu, H. Zhang, J. Hu, Electrochem. Commun. 9 (2007) 2643–2648.
[25] M.-H. Shao, K. Sasaki, R.R. Adzic, J. Am. Chem. Soc. 128 (2006) 3526–3527.
[26] V. Jalan, E.J. Taylor, J. Electrochem. Soc. 130 (1983) 2299–2302.
[27] S. Mukerjee, S. Srinivasan, M.P. Soriaga, J. Electrochem. Soc. 142 (1995) 1409–1422.
[28] U.A. Paulus, T.J. Schmidt, H.A. Gasteiger, R.J. Behm, J. Electroanal. Chem. 495 (2001) 134–145.
[29] J. Souza-Garcia, V. Climent, J.M. Feliu, Electrochem. Commun. 11 (2009) 1515–1518.
[30] O. Savadogo, K. Lee, K. Oishi, S. Mitsushima, N. Kamiya, K.I. Ota, Electrochem. Commun. 6 (2004) 105–109.
[31] J. Hu, H. Zhang, L. Gang, Energy Convers. Manage. 49 (2008) 1019–1027.
[32] Z. Xie, S. Holdcroft, J. Electroanal. Chem. 568 (2004) 247–260.